Proceedings of the Sixth International Conference on
Railway Technology: Research, Development and Maintenance
Edited by: J. Pombo
Civil-Comp Conferences, Volume 7, Paper 6.2
Civil-Comp Press, Edinburgh, United Kingdom, 2024
ISSN: 2753-3239, doi: 10.4203/ccc.7.6.2

Evaluation of ballast loading in a crossing

S. Gapp[1], D. Samardzic[1], J. Maierhofer[1], W. Daves[1], M. Pötz[2] and C. Ebner-Mürzl[2]

[1]Materials Center Leoben Forschung GmbH, Leoben Austria
[2]voestalpine Railway Systems GmbH, Zeltweg Austria

Abstract

Switches and crossings are key components of a railway network because they enable track flexibility. However, they are also critical parts regarding safe operations. High dynamic loads at the wheel/rail interface lead to higher damage rates which increase operating costs and life cycle costs. Track settlement and ballast degradation are mainly driven by sleeper forces and sleeper movements. They are critical issues in railway engineering, affecting safety and efficiency. The ballast loading during wheel transition is evaluated using a finite element model and results of a measurement campaign on an Austrian railway turnout. The crossing's performance is evaluated using displacement sensors installed on the sleeper in the transition zone. A test run with a Siemens ER 2016 diesel-electric locomotive was conducted to validate the finite element model. The simulation shows the wheel/rail contact forces during the transition and the influence on the sleeper movement which is delayed due to the system's dynamic properties. From these results, the ballast loading is determined. It is shown that the elastic support of the crossing reduces the dynamic load transfer to the ballast significantly.

Keywords: turnout, switches and crossings, crossing, finite element simulation, ballast loading, sleeper displacement

1 Introduction

The ability to navigate between different rail tracks is facilitated by switches and crossings (S&C). These components play a key role in increasing the flexibility of a

railway network. However, the installation of S&C introduces discontinuities in the track, resulting in exceptionally high dynamic loads at the wheel/rail interface [1]. The recurrent rolling sliding contact between the wheel and rail induces three primary damage mechanisms: wear, plastic deformation and rolling contact fatigue (RCF) [2]. As a result of the dynamically caused peak loads the damage rates are increased compared to the main line track. In addition, the contact conditions and the resulting damage are influenced by geometrical changes due to plastic deformation of the contact partners [3]. The need to maintain the turnout safety requires frequent inspections and maintenance intervals, resulting in increased operating costs and consequently increased life cycle costs (LCC) [4].

The dynamic impact that occurs as the wheel transitions from the wing rail to the crossing nose, as depicted in Figure 1, introduces high stresses, varying rolling radii (slip) and high dynamic normal and lateral loads Figure 1 [5]. These challenging conditions require the use of highly engineered materials. Premium rail steels, such as ultra-fine pearlitic or Hadfield steels, are used to withstand these demanding loads, thereby extending maintenance intervals and reducing the LCC of these critical railway components. [6]

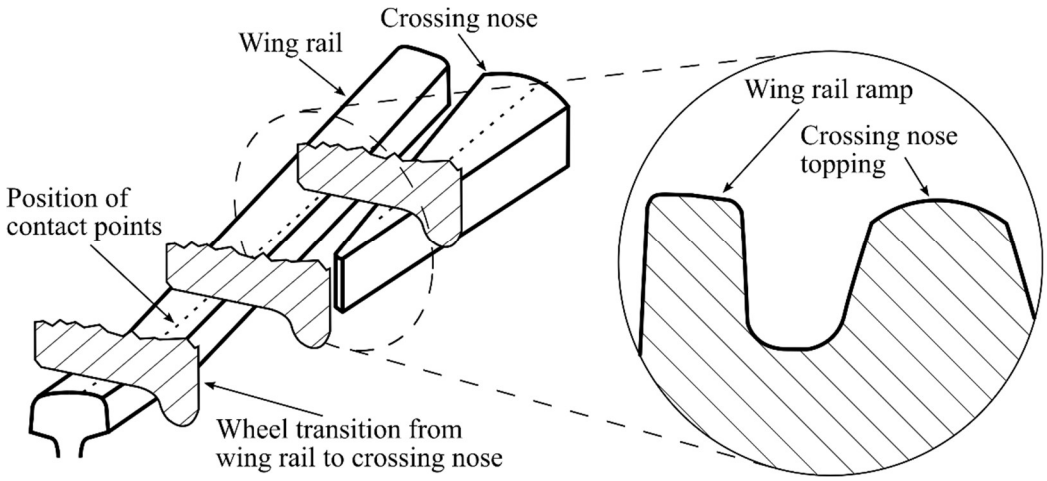

Figure 1: Wheel transition from the wing rail to the crossing nose based on [7].

Ballast deformation (track settlement) and degradation is a complex process influenced by various parameters and environmental conditions. From a dynamical point of view, two parameters of loads and sleeper movements, respectively, drive damage evolution in the ballast. These are the amplitude and frequency of the load [8]. Particle crushing is enhanced by high dynamical loadings, which occur in turnouts [9]. If ballast particles crush, the ability of ballast movement is decreased and so-called fouling may occur [10, 11]. From an environmental aspect water infiltration, which is favoured by ballast fouling, followed by possible saturation decrease the load-bearing capacity [12]. Since the environmental conditions are out of scope of this paper, these influences are not considered.

Both ballast degradation and track settlement are major concerns in railway engineering, as they affect the safety and efficiency of the railway infrastructure.

Regular inspection, maintenance, and replacement of degraded ballast is essential to ensure long-term track performance. [13] Therefore, the scope of this paper is the evaluation of ballast loading under the crossing nose during the wheel transition.

2 Methods

To evaluate the ballast loading during the wheel transition, two parts of work are performed. First, a finite element (FE) is developed. Second, a measurement campaign is conducted on this particular turnout and used for validation of the simulation.

2.1 Finite Element model

A finite element model of a particular crossing that has been installed in the Austrian railway network is developed. For the development and calculation the commercial software package Abaqus 2019 [14] is used. The model consists of a single S1002 wheel that rolls over the comprehensive crossing and simulates the transition of the wheel from the wing rail to the crossing nose. Therefore, this is a half-track model, which is common for such time consuming and complex models, e.g. [15–18]. The FE model contains approximately 850 000 hexahedral (C3D8R) and 220 000 tetrahedral (C3D10M) elements. The hexahedral elements are applied in the wheel/rail contact area, since these elements are a good choice for contact calculations [14]. In order to account for the complex geometry of the crossing, tetrahedral elements are applied in the non-contact region. These regions are meshed rather coarsely, but fine enough to accurately represent the stiffness and mass of the demonstrator. The model of the crossing includes the inner cast structure accounting for its optimized mass distribution. An overview of the model is given in Figure *2*.

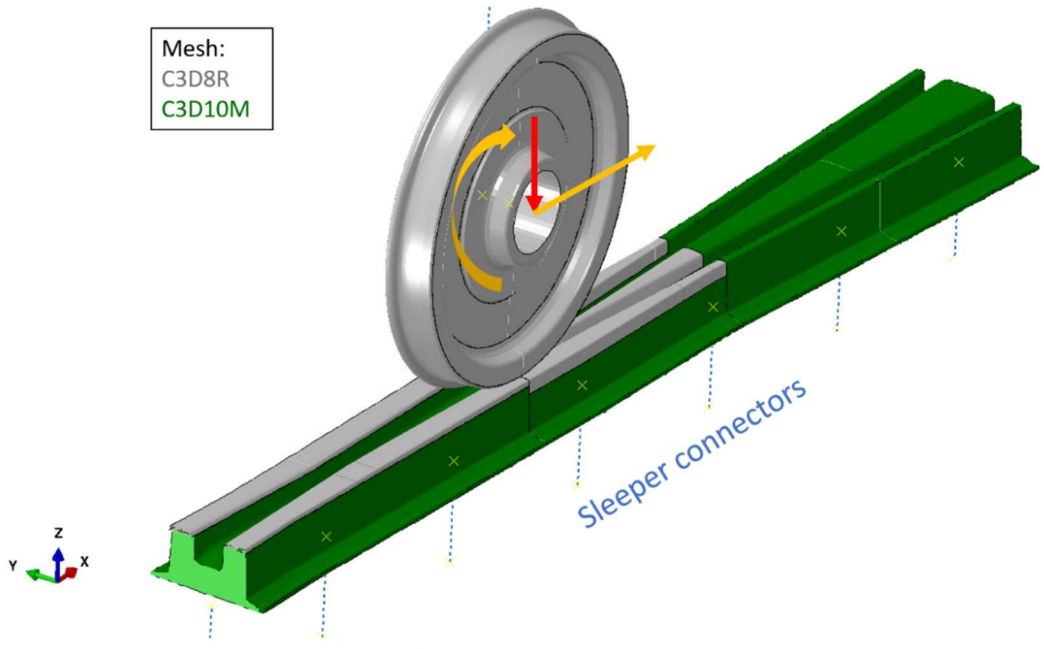

Figure 2: 3D Finite element model of the crossing.

The explicit simulation shows a standard S1002 wheel with 10 000 kg of mass applied via spring-damper combination rolling over the crossing in the through direction at a speed of 33.33 m/s (= 120 km/h), see Figure 3. The rolling radius of the wheel is 0.5 m. This setup is based on a Siemens ER20 locomotive that rolled over the turnout during the measurement campaign, see section 2.2. To depict the unsprang mass of the system correctly the half axle mass is applied as point mass (the mass of the wheel considered by its volume and density). The load is applied by gravity with a value of 9.81 m/s².

The first impact on the crossing nose during the wheel transition is of particular interest. The wheel is fixed laterally and can move both longitudinally and vertically. The wheel is initially subjected to a rotational speed of 66.67 rad/s and a translational speed of 33.33 m/s. According to the real layout of the demonstrator, seven sleepers are connected to the bottom of the crossing. They are represented by mass points, spring and damper connectors. With the selected output ratio, the result data rate is 12.8 kHz.

The dynamical behaviour of the fastening system (clips, pads, etc.) which connects the crossing with the sleepers is modelled with spring and damper elements. The sleepers, which are represented by point masses, are again connected with spring and damper elements in downward direction to consider the ballast including under-sleeper-pads. This setup has been chosen to account for the influence of the specific masses of the parts and their interaction. The finite element model is shown in Figure 3. Several parameters that are used for this simulation are summarized in Table 1. Elastic material models are applied. The wheel material has a Young's modulus E of 210 GPa and a Poisson ratio ν of 0.3. For the crossing a Young's modulus E of 206 GPa is applied.

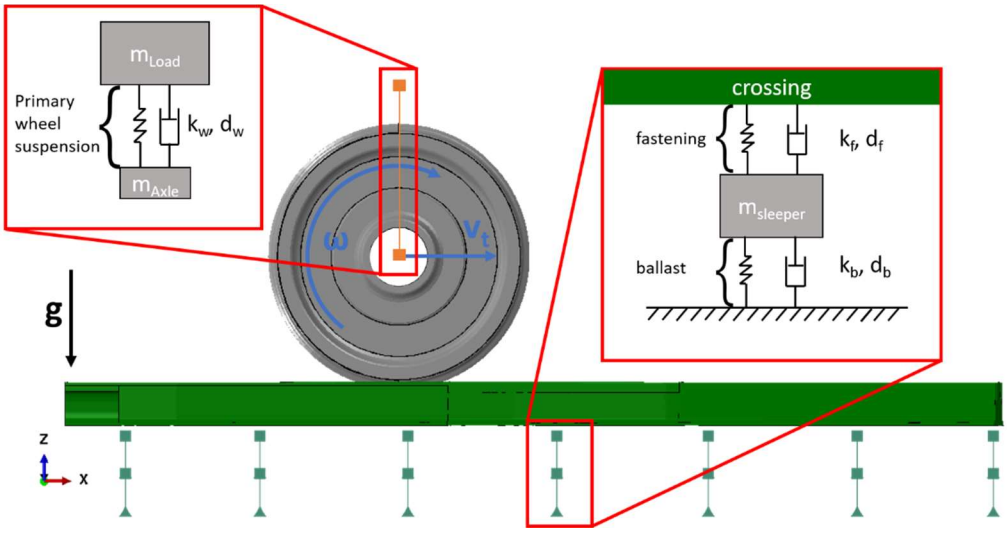

Figure 3: FE model of the crossing with a detailed view of modelled track bed.

Parameter	Symbol	Value
Vehicle mass	m_{Load}	10 000 kg
Axle mass	m_{Axle}	478.5 kg
Sleeper mass	$m_{Sleeper}$	239 – 253 kg
Spring stiffness of the primary wheel suspension	k_w	1.22 MN/m
Damping coefficient of the primary wheel suspension	d_w	30 kNs/m
Spring stiffness of the fastening system	k_f	33.25 MN/m
Damping coefficient of the fastening system	d_f	5 kNs/m
Spring stiffness of the ballast	k_b	30 MN/m
Damping coefficient of the ballast	d_b	75 kNs/m
Train speed	v_t	33.33 m/s
Rotational wheel velocity	ω	66,67 rad/s
Gravity	g	9.81 m/s²

Table 1: Parameters for the FE simulation.

2.2 Measurement approach

The turnout is installed in Austria near to Vienna. To evaluate the performance of this turnout, several sensors are implemented on different parts of the turnout. The crossing is made of Hadfield steel and explosive depth hardened. One part of the In2Track3 project is the evaluation of the ballast loading via ballast deflection. Therefore, the sleeper in the transition zone is equipped with displacement sensors, see Figure 4. The output rate of these sensors is 2 kHz.

Figure 4: Installed sleeper displacement sensor to measure the ballast deflection.

Figure 4 visualises the installation setup of the sensors. Two baseplates are placed on the ballast and connect via a horizontal beam, therefore, the relative, vertical displacement of the sleeper with respect to the ballast is measured. The displacement sensor is mounted on this beam and connected with the top surface of the sleeper. The displacement sensors are positioned in the middle of rail and crossing. One is installed in the through and one in the diverging direction, as shown in Figure 5.

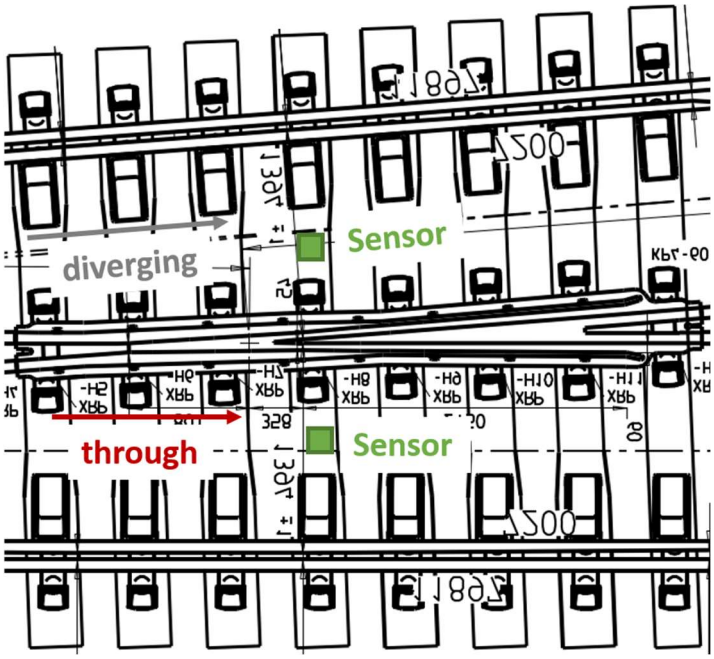

Figure 5: Sensor positions in track.

For the purpose of defined conditions, a test run with a single Siemens ER 2016 diesel-electric locomotive has been carried out. This locomotive has a total mass of about 80 tonnes. The locomotive ran in the through direction of the turnout with a speed of 120 km/h.

3 Results

The load transition from the wheel into the ballast is evaluated via the sleeper displacements. Simulation results are validated with sensor data from field. In the following diagrams, the longitudinal position 0 corresponds to the theoretical crossing point (TCP).

In Figure 6, the measured and calculated sleeper displacements are compared. The dotted grey lines represent the actual sensor data. The black line is the mean curve derived from the sensor data. Since the sensors are placed in between rail and crossing this approach is chosen to represent the displacement directly beneath the crossing. The first phase (from 0.15 to 0.4 m) shows a nearly constant displacement. This is followed by an upward movement of the sleeper, which represents an unloading of the sleeper and consequently the ballast. This might be unexpected at first but due to the shape of the conical wheel, the inclined running surface of the wing rail towards

the crossing nose, see Figure 1, and a kink of the wing rail, indicated in Figure 6, the wheel has to move downwards [19, 20]. Due to its inertia, the wheel cannot follow this change directly, therefore, the sleeper is unloaded and moves upwards. This upward movement is followed by a downward movement of the sleeper that results from the wheel impact on the crossing nose. The measured, maximum relative displacement between sleeper and ballast amounts to 0.58 mm, as shown in Figure 6.

The red curve accounts for the calculated sleeper displacement. In the simulation, the first contact of the wheel with the wing rail leads to a dynamic bouncing of the wheel. This is the reason for the transient response within 0.3 m from TCP. Comparable to the measurement, a plateau is reached and followed by a raise of the sleeper. The value of this upward movement is lower than the measured value in track. However, the downward movement, which is initiated by the wheel impact on the crossing nose, is in good agreement with the sensor data both amplitude and frequency.

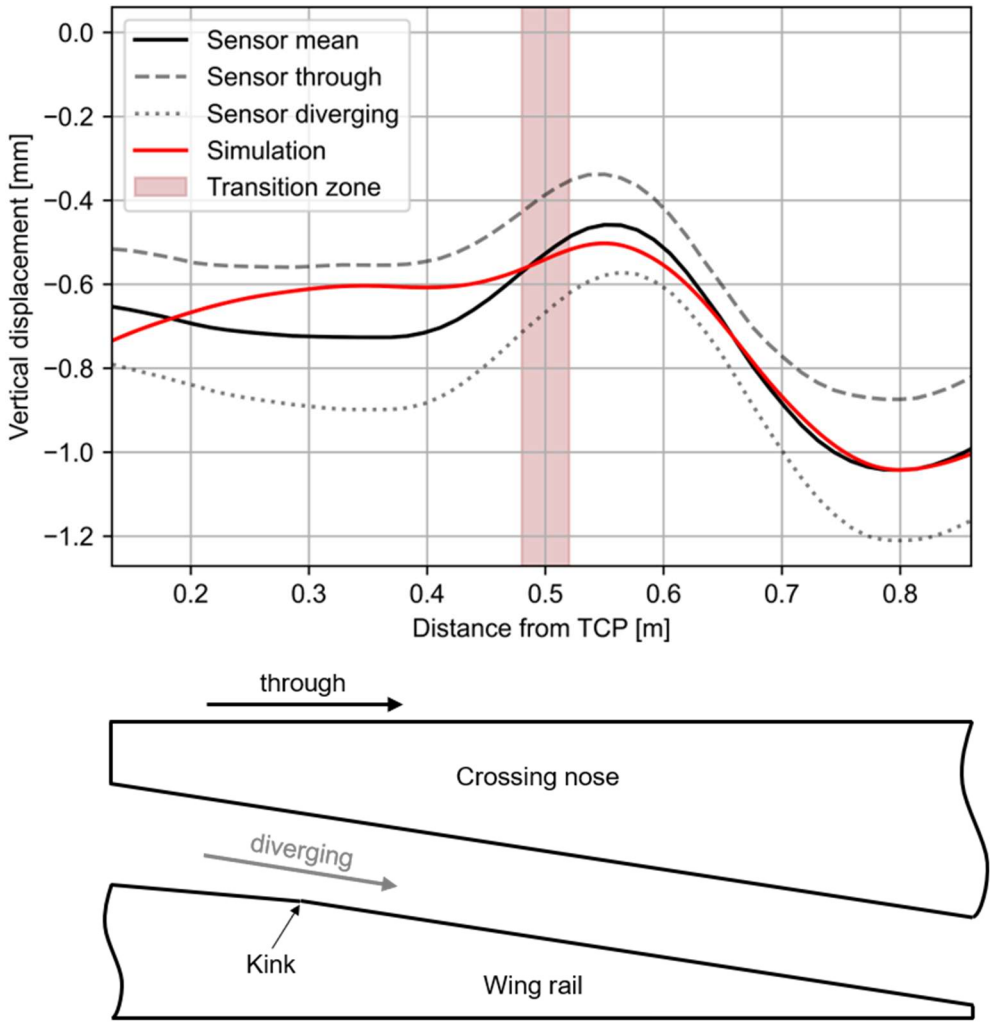

Figure 6: Comparison of the calculated and measured sleeper displacements during the wheel transition.

Figure 7 shows the calculated wheel/rail contact forces during the wheel transition and the corresponding sleeper forces on the ballast. The contact force between wheel and wing rail indicates the previously mentioned unloading before the transition (orange line from 0.3 to 0.42 m). Due to the inertias and damping properties of the system, the sleeper movement is delayed compared to the time of maximum contact forces. While the wheel is gaining full contact with the wing rail again, and therefore the contact force is increasing (0.42 to 0.48 m from TCP), the first contact with the crossing nose happens. The wheel transition, the distance where the wheel is in contact simultaneously with wing rail and crossing nose, amounts from 0.48 to 0.52 m from the TCP. Afterwards, the wheel runs solely on the crossing nose. The contact force on the crossing nose (blue curve) shows two peaks. However, the sleeper force is reacting to the dynamic contact forces in a delayed and significantly reduced manner. This is due to the dynamic properties (springs, dampers and inertias) of the parts.

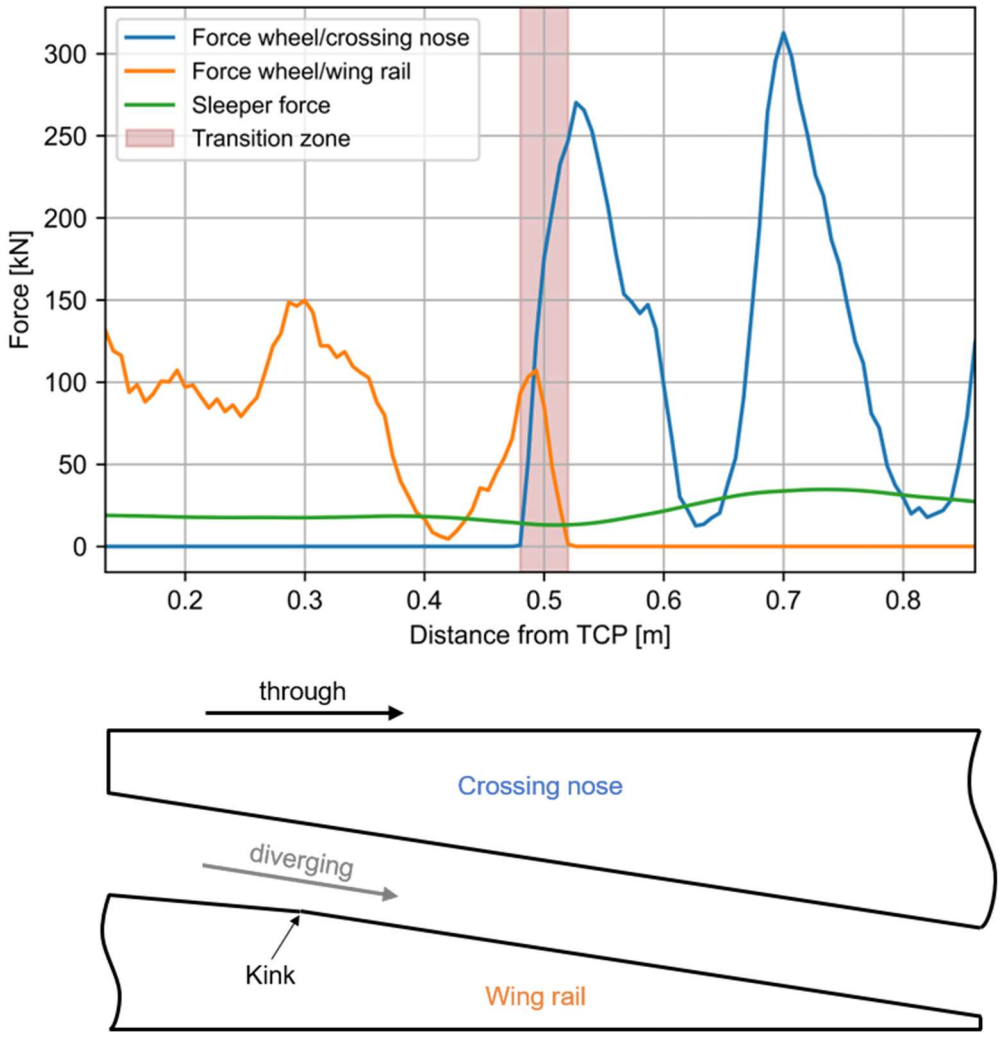

Figure 7: Calculated sleeper forces during the wheel transition from the wing rail to the crossing nose.

4 Conclusions and Contributions

The FE model of the crossing nose and the wing rails simulates a wheel transition on an instrumented turnout that is installed in the Austrian Federal Railways. The model represents the measured behaviour of this crossing with special regards to the sleeper movements sufficiently accurate.

The comparison of calculated and measured sleeper displacements, which is presented in Figure 6, leads to the following conclusions:

- The absolute unloading displacement of the sleeper (0.4 – 0.55 m from TSP), that happens before the transition of the wheel to the crossing nose is slightly underestimated.
- The absolute downward movement of the sleeper due to the impact of the wheel on the crossing nose (0.55 -0.8 m from TSP) is represented in an accurate and quantitative manner.

This comparison validates the simulation results. The evaluation of contact and sleeper forces in Figure 7 reveals that the elastic support of the crossing (fastening system and ballast) reduces the dynamic load transfer to the ballast significantly.

Acknowledgements

The authors gratefully acknowledge the financial support under the scope of the COMET program within the K2 Center “Integrated Computational Material, Process and Product Engineering (IC-MPPE)” (Project No 886385). This program is supported by the Austrian Federal Ministries for Climate Action, Environment, Energy, Mobility, Innovation and Technology (BMK) and for Labour and Economy (BMAW), represented by the Austrian Research Promotion Agency (FFG), and the federal states of Styria, Upper Austria and Tyrol.

This work was financially supported by European Union’s Horizon 2020 Programme Research and Innovation action under Grant Agreement No 101012456 (Project In2Track3).

References

[1] J. Wiedorn, W. Daves, U. Ossberger, H. Ossberger, and M. Pletz, "Simplified explicit finite element model for the impact of a wheel on a crossing – Validation and parameter study," *Tribology International*, vol. 111, pp. 254–264, 2017, doi: 10.1016/j.triboint.2017.03.023.

[2] I. Grossoni, P. Hughes, Y. Bezin, A. Bevan, and J. Jaiswal, "Observed failures at railway turnouts: Failure analysis, possible causes and links to current and future research," *Engineering Failure Analysis*, vol. 119, p. 104987, 2021, doi: 10.1016/j.engfailanal.2020.104987.

[3] M. Pletz, W. Daves, W. Yao, W. Kubin, and S. Scheriau, "Multi-scale finite element modeling to describe rolling contact fatigue in a wheel–rail test rig," *Tribology International*, vol. 80, pp. 147–155, 2014, doi: 10.1016/j.triboint.2014.07.005.

[4] A. Johansson *et al.,* "Simulation of wheel–rail contact and damage in switches & crossings," *Wear*, vol. 271, 1-2, pp. 472–481, 2011, doi: 10.1016/j.wear.2010.10.014.
[5] J. Wiedorn, W. Daves, H. Ossberger, and M. Pletz, "A Simplified Dynamic Finite Element Model for the Impact of a Wheel on a Crossing: Validation and Parameter Study," in *Proceedings of the Third International Conference on Railway Technology: Research, Development and Maintenance*, Cagliari, Sardinia, Italy, 2016.
[6] R. Stock and R. Pippan, "RCF and wear in theory and practice—The influence of rail grade on wear and RCF," *Wear*, vol. 271, 1-2, pp. 125–133, 2011, doi: 10.1016/j.wear.2010.10.015.
[7] Y. Cao, W. Zhao, Y. Lin, K. Yao, and X. Lin, "Dynamic optimization of the rail-crown geometry in the rigid crossing area by controlling the position of the wheel-load transition," *Proceedings of the Institution of Mechanical Engineers, Part F: Journal of Rail and Rapid Transit*, vol. 234, no. 9, pp. 1017–1028, 2020, doi: 10.1177/0954409719882501.
[8] Q. D. Sun, B. Indraratna, and S. Nimbalkar, "Deformation and Degradation Mechanisms of Railway Ballast under High Frequency Cyclic Loading," *J. Geotech. Geoenviron. Eng.*, vol. 142, no. 1, 2016, doi: 10.1061/(ASCE)GT.1943-5606.0001375.
[9] S. Lobo-Guerrero and L. E. Vallejo, "Discrete Element Method Analysis of Railtrack Ballast Degradation during Cyclic Loading," *Granular Matter*, vol. 8, 3-4, pp. 195–204, 2006, doi: 10.1007/s10035-006-0006-2.
[10] R. Bruzek, T. D. Stark, S. T. Wilk, H. B. Thompson, and T. R. Sussmann, "Fouled Ballast Definitions and Parameters," in *2016 Joint Rail Conference*, Columbia, South Carolina, USA, 2016.
[11] D. Ionescu, "Ballast Degradation and Measurement of Ballast Fouling, 7th Railway Engineering Proceedings, 5-6 July," *London, UK*, pp. 169–180, 2004.
[12] H. Faghihi Kashani, C. L. Ho, and J. P. Hyslip, "Fouling and water content influence on the ballast deformation properties," *Construction and Building Materials*, vol. 190, pp. 881–895, 2018, doi: 10.1016/j.conbuildmat.2018.09.058.
[13] J. C. O. Nielsen, E. G. Berggren, A. Hammar, F. Jansson, and R. Bolmsvik, "Degradation of railway track geometry – Correlation between track stiffness gradient and differential settlement," *Proceedings of the Institution of Mechanical Engineers, Part F: Journal of Rail and Rapid Transit*, vol. 234, no. 1, pp. 108–119, 2020, doi: 10.1177/0954409718819581.
[14] Dassault Systèmes, *SIMULIA User Assistance R2019x*: Dassault Systèmes, 2019. Accessed: Apr. 7 2023. [Online]. Available: www.3ds.com
[15] D. Velic, M. Krobath, E. Stocker, U. Ossberger, J. Gsodam, and W. Daves, "A finite element modelling approach for the numerical analysis of switch rail contact loading and cyclic profile degradation," *Proceedings of the Institution of Mechanical Engineers, Part F: Journal of Rail and Rapid Transit*, 095440972210956, 2022, doi: 10.1177/09544097221095694.
[16] J. Wiedorn, W. Daves, U. Ossberger, H. Ossberger, and M. Pletz, "Finite element model for predicting the initiation of subsurface damage in railway crossings—A parametric study," *Proceedings of the Institution of Mechanical Engineers,*

Part F: Journal of Rail and Rapid Transit, vol. 233, no. 6, pp. 614–628, 2019, doi: 10.1177/0954409718797039.

[17] G. Schnalzger, S. Gapp, U. Ossberger, C. Bucher, T. Antretter, W. Daves, "Wear and RCF assessment in switch rails for different materials", in J. Pombo, (Editor), "Proceedings of the Fifth International Conference on Railway Technology: Research, Development and Maintenance", Civil-Comp Press, Edinburgh, UK, Online volume: CCC 1, Paper 5.9, 2022, doi:10.4203/ccc.1.5.9

[18] G. Schnalzger *et al.,* "Simplified Damage Assessment Tool for Rails and Crossings Based on Standard Wear and RCF Models," *Metals*, vol. 12, no. 12, p. 2169, 2022, doi: 10.3390/met12122169.

[19] B. A. Pålsson, "Optimisation of railway crossing geometry considering a representative set of wheel profiles," *Vehicle System Dynamics*, vol. 53, no. 2, pp. 274–301, 2015, doi: 10.1080/00423114.2014.998242.

[20] J. Wiedorn, W. Daves, U. Ossberger, H. Ossberger, and M. Pletz, "Numerical assessment of materials used in railway crossings by predicting damage initiation – Validation and application," *Wear*, 414-415, pp. 136–150, 2018, doi: 10.1016/j.wear.2018.08.011.